Available online at www.sciencedirect.com
SCIENCE DIRECT
Remote Sensing of Environment 102 (2006) 293–305
Remote Sensing of Environment
www.elsevier.com/locate/rse

Estimation of evaporative fraction from a combination of day and night land surface temperatures and NDVI: A new method to determine the Priestley–Taylor parameter

Kaicun Wang [a,b,c,*], Zhanqing Li [b], M. Cribb [b]

[a] Laboratory for Middle Atmosphere and Global Environment Observation (LAGEO), Institute of Atmospheric Physics, Chinese Academy of Sciences, Beijing, 100029, PR China
[b] Earth System Science Interdisciplinary Center (ESSIC) and Department of Atmospheric and Oceanic Science, University of Maryland, College Park, Maryland, MD 20742, USA
[c] State Key Laboratory of Remote Sensing, Joint sponsored by Institute of Remote Sensing Applications of Chinese Academy of Sciences and Beijing Normal University, P. R. China

Received 19 September 2005; received in revised form 8 February 2006; accepted 10 February 2006

Abstract

Satellite remote sensing is a promising technique to estimate global or regional evapotranspiration (ET) or evaporative fraction (EF) of the surface total net radiation budget. The current methods of estimating the ET (or EF) from the gradient between land surface temperature (T_s) and near surface air temperature are very sensitive to the retrieval errors of T_s and the interpolation errors of air temperature from the ground-based point measurements. Two types of methods have been proposed to reduce this sensitivity: the thermal inertia method and the T_s–normalized difference vegetation index (NDVI) (T_s–NDVI) spatial variation method. The former is based on the temporal difference between T_s retrievals, and the latter uses the spatial information of T_s. Another approach is proposed here that combines the advantages of the two types of methods and uses day–night T_s difference–NDVI (ΔT_s–NDVI). Ground-based measurements collected by Energy Balance Bowen Ratio systems at the 11 enhanced facilities located at the Southern Great Plains of the United States from April 2001 to May 2005 were analyzed to identify parameterization of EF. ΔT_s–NDVI spatial variations from the Aqua and Terra MODerate-resolution Imaging Spectroradiometer (MODIS) global daily products, at 1 km resolution were used to estimate EF. Ground-based measurements taken during 16 days in 2004 were used to validate the MODIS EF retrievals. The EFs retrieved from the spatial variations of ΔT_s–NDVI show a distinct improvement over that retrieved from the ΔT_s–NDVI. The EF can be retrieved with a mean relative accuracy of about 17% with the proposed ΔT_s–NDVI spatial variations.

Keywords: Evaporative fraction (EF); MODIS; Southern Great Plains (SGP); Land surface temperature; Normalized difference vegetation index (NDVI)

1. Introduction

Evapotranspiration (ET) is a primary process driving the energy and water exchange between the hydrosphere, atmosphere and biosphere (e.g. Priestley & Taylor, 1972; Monteith, 1973). It is required by short-term numerical weather predication models and longer-term simulation for climate predication (Rowntree, 1991). Different methods have been proposed for measuring ET on various spatial scales from individual plants (i.e. sap-flow, porometer, lysimeter) (Yunusa et al., 2004), to fields (i.e. field water balance, Bowen ratio, scintillometer) (Brotzge & Kenneth, 2003) or landscape scales (i.e. eddy correlation and catchment water balance) (Baldocchi et al., 2001).

However, conventional techniques provide essentially point measurements, which usually do not represent areal means because of the heterogeneity of land surfaces and the dynamic nature of heat transfer processes. Satellite remote sensing is a promising tool which has been used to provide reasonable estimates of the evaporative fraction (EF) defined as the ratio of

* Corresponding author. LAGEO, Institute of Atmospheric Physics, Chinese Academy of Sciences, Beijing, 100029, P. R. China. Tel.: +86 10 82080871; fax: +86 10 82080863.
E-mail addresses: wangkaicun@mail.iap.ac.cn, wangkaicun@hotmail.com (K. Wang).

0034-4257/$ - see front matter © 2006 Elsevier Inc. All rights reserved.
doi:10.1016/j.rse.2006.02.007

ET to available total energy (Shuttleworth et al., 1989). Over the last few decades, a large number of techniques have been proposed to estimate EF (Wang et al., 2005d; Verstraeten et al., 2005).

Under the assumption that the energy storage by the canopy is negligible, ET (also denoted as λE) can be calculated as a residual of the surface available energy (R_n), the sensible heat flux (H) and ground heat flux (G):

$$\lambda E = R_n - G - H \quad (1)$$

Surface heat flux H is usually determined following the Monin–Oblukhov similarity theory (Monin & Oblukhov, 1954) in the following parameterized form (e.g., Friedl, 2002; Wang et al., 2005d for review):

$$H = \frac{\rho C_p (T_0 - T_a)}{r_a} \quad (2)$$

where ρ the density of air, C_p is the specific heat of air, T_0 is the surface aerodynamic temperature, T_a is the near surface air temperature, and r_a is the aerodynamic resistance. In satellite remote sensing applications, the land surface radiometric temperature (T_s) retrieval is often used instead of the aerodynamic temperature in Eq. (2) (see, for example, Kustas et al., 1989), despite numerous uncertainties associated with the retrieval of T_s (e.g. Prata & Cechet, 1999; Wang et al., 2005a).

Attempts have been made to use the temporal variation of T_s to reduce the sensitivity of ET retrievals to the uncertainties in T_s (Albellaoui et al., 1986; Anderson et al., 1997; Caparrini et al., 2004; Norman et al., 2000). The thermal inertia method is one of the approaches used. Thermal inertia is a bulk property and is a measure of resistance of a material to changes in temperature (Price, 1977). For a given heat flow, a high thermal inertia leads to a small change in temperature (Pratt & Ellyett, 1979). Different surface cover types have different thermal inertia and soil thermal inertia mainly depends on soil moisture content. Thermal inertia derived from satellite data has been used to determine soil moisture (Pratt & Ellyett, 1979), ET (Albellaoui et al., 1986), and crop water stress (Price, 1982). However, early models to calculate thermal inertia from satellite data still require many parameters (i.e., average wind speed, surface roughness, average temperature of air and ground surface, etc.), which have to be obtained from ground-based measurements (Sobrino & EL Kharraz, 1999).

The T_s and NDVI spatial variation (T_s–NDVI) method uses spatial information of the T_s and NDVI to reduce the requirement of accuracy of T_s retrievals (Venturini et al., 2004). The spatial variation of T_s and NDVI often results in a triangular shape, with lower temperature for wet, vegetated surfaces (cold edge of shape) and higher temperature for dry surface (warm edge) (Carlson et al., 1994; Price, 1990), or a trapezoid shape (Moran et al., 1994) if a full range of fractional vegetation cover and soil moisture content is represented in the data. The approach of using the T_s–NDVI spatial variation to obtain EF has been validated using land surface models simulations (Carlson et al., 1995; Friedl, 2002; Gillies et al., 1997; Gowarda et al., 2002). Several studies focus on the slope of the T_s/NDVI spatial variation (e.g., Friedl & Davis, 1994; Nemani & Running, 1989; Smith & Choudhury, 1991). Water stress index or drought index were determined successfully from the T_s–NDVI spatial variation (Sandholt et al., 2002; Wan et al., 2004a).

Jiang and Islam (2001) estimated EF by interpolating the Priestley–Taylor parameter (Priestley & Taylor, 1972) using the triangular distribution of the T_s–NDVI spatial variation. EF is parameterized as a function of the Priestley–Taylor parameter, α, and the air temperature controlling factor $\Delta/(\Delta+\gamma)$ (see Section 3 for details). Recently, a similar spatial variation of broadband albedo and T_s (T_s–albedo) was proposed to estimate EF (Gómeza et al., 2005; Roerink et al., 2000; Su et al., 1999; Verstraeten et al., 2005). However, some methods do not include $\Delta/(\Delta+\gamma)$ and have different parameterization of α and EF (Gómeza et al., 2005; Roerink et al., 2000; Su et al., 1999; Verstraeten et al., 2005).

We propose a method employing day–night differences and NDVI (ΔT_s–NDVI). The objectives of this study are: (1) to extensively explore the utility of the data to further our understanding of parameters dictating the variation of EF to select proper parameterization of EF; and (2) to evaluate and improve a remote sensing method for estimating EF.

2. Data

Given that satellite can only provide limited information pertaining to ET (or EF), a major task in the remote sensing of ET (or EF) is to identify key factors influencing the processes involved and its parameterization from satellite data. To this end, extensive measurements of surface fluxes, meteorological and soil variables, as well as coincident satellite data are required. This requirement is met thanks to the continuous observations made over the past decade at the Southern Great Plains site under the aegis of the Atmospheric Radiation Measurement (ARM) Program. Fourteen Energy Balance Bowen Ration (EBBR) systems were deployed to measure the ET, the EF and related meteorological parameters (e.g. the air temperature and the wind speed), as well as the soil moisture. These ground measurements are available at http://www.archive.arm.gov/. The MODIS land surface products related to ET, including land surface temperature, vegetation indices, albedo, and land cover type (http://www.edcdaac.usgs.gov/modis/dataprod.html) are also used in this study. The two data sets cover a period ranging from April 2001 to May 2005.

Two MODIS instruments (Salomonson et al., 1989) have been launched for global studies of the atmosphere, land, and ocean processes. The first instrument was launched on 18 December 1999 on a morning platform called Terra, and the second was launched on 4 May 2002 on an afternoon platform called Aqua. The Terra overpass time is around 10:30 AM (local solar time) in its descending mode and 10:30 PM in its ascending mode. The Aqua overpass time is around 1:30 PM in its ascending mode and 1:30 AM in its descending mode.

Three MODIS land products are used in this study: the 96-day land cover product, the 16-day vegetation indices product and the daily T_s product at 1-km resolution. Two algorithms

were used to retrieve T_s from the MODIS thermal and middle infrared spectral regions: the generalized split window algorithm (Wan & Dozier, 1996) and the MODIS day/night land surface temperature algorithm (Wan & Li, 1997). The product at 1-km resolution produced by the former algorithm (MOD11A1 for Terra MODIS or MYD11A1 for Aqua MODIS) is selected because of its higher accuracy (1 K) (Wan et al., 2002, 2004b, Wang et al., 2005a). Independent validation experiments show that the MODIS T_s produced by split-window algorithm agrees well with the ground measurements of T_s, with differences comparable or less than the uncertainties of the ground measurements for most of the days (bias of +0.1 °C and standard deviation of 0.6 °C, for cloud-free cases and viewing angle less than 60°) (Coll et al., 2005).

Two indices were used from the MODIS global vegetation indices products: the NDVI and the Enhanced Vegetation Indices (EVI) (Huete et al., 2002). In this study, NDVI was selected because it is the more widely accepted index. Nagler et al. (2005a,2005b) argued that EVI was a better predictor of ET than NDVI when using empirical formula to estimate ET at multiple riparian sites. We also used EVI to retrieve EF but found no substantial differences from those estimated using the NDVI. Eq. (A1) in Appendix A shows EF retrievals are not sensitive to vegetation indices using the method proposed.

The Southern Great Plains (SGP) Cloud and Radiation Testbed (CART) region spans over a 350-km by 400-km domain across portions of south-central Kansas and north-central Oklahoma. Fourteen enhanced facility sites instruments with Energy Balance Bowen Ratio (EBBR) stations are located throughout the SGP CART region and most of the sites fall within the MODIS land products tile number H10V5. Of the 14 EBBR sites, data from 3 sites were not selected because one site was vacated in April 2002 (EF25), another site (EF26) lies within a different MODIS land products tile and the EF27 site only became operational in May 2003. Fig. 1 shows the International Geosphere–Biosphere Programme (IGBP) land cover types that characterize the study region, with water bodies shown in black, and the superimposed locations of the 11 enhanced facility sites chosen for this study. Fig. 1 shows that the surface around sites EF04 and EF08 is more heterogeneous than that of other sites. Table 1 shows that the 11 sites chosen represent a variety of land types, soil moisture and vegetation conditions.

These stations operate continuously throughout the year. Meteorological data collected by the EBBR stations are used to

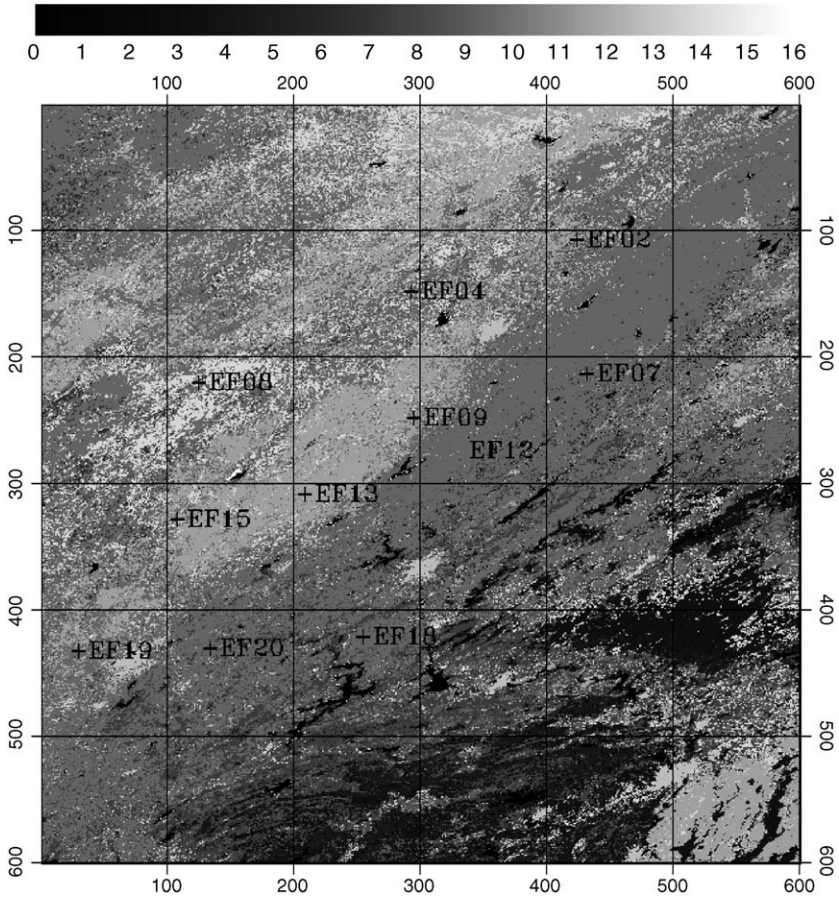

Fig. 1. The different land cover types characterizing the South Great Plains study region. The pixel resolution is about 1 km and the whole region is about 550 × 550 km^2. International Geosphere–Biosphere Programme (IGBP) land cover types were shown in the figure: (0) water body, (1) evergreen needleleaf forest, (2) evergreen broadleaf forest, (3) deciduous needleleaf forest, (4) deciduous broadleaf forest, (5) mixed forest, (6) closed shrubland, (7) open shrubland, (8) woody savanna, (9) savanna, (10) grassland, (11) permanent wetland, (12) crop land, (13) urban/build up, (14) crop land/natural vegetation mosaic, (15) snow/ice, and (16) barren lands. The locations of the 11 enhanced facility sites are also shown.

Table 1
Brief description of the 11 enhanced facilities located throughout the Southern Great Plains

Site	Lat./Long.	Elevation (m)	Land cover	Mean (Max) NDVI	Mean ET (EF)	Mean SM
Hillsboro, Kansas: EF02	38.305′N, 97.301′W	447	Grass	0.51 (0.74)	124.9 (0.535)	0.232
Plevna, Kansas: EF04	37.953′N, 98.329′W	513	Rangeland (ungrazed)	0.43 (0.69)	87.4 (0.363)	0.088
Elk Falls, Kansas: EF07	37.383′N, 96.180′W	283	Pasture	0.49 (0.74)	137.9 (0.648)	0.238
Coldwater, Kansas: EF08	37.333′N, 99.309′W	664	Rangeland (grazed)	0.36 (0.67)	103.4 (0.436)	0.084
Ashton, Kansas: EF09	37.133′N, 97.266′W	386	Pasture	0.49 (0.74)	130.6 (0.545)	0.205
Pawhuska, Oklahoma: EF12	36.841′N, 96.427′W	331	Native prairie	0.48 (0.81)	122.4 (0.500)	0.240
Lamont, Oklahoma: EF13	36.605′N, 97.485′W	318	Pasture and wheat	0.51 (0.79)	115.2 (0.493)	0.192
Ringwood, Oklahoma: EF15	36.431′N, 98.284′W	418	Pasture	0.41 (0.62)	112.3 (0.481)	–
Morris, Oklahoma: EF18	35.687′N, 95.856′W	217	Pasture (ungrazed)	0.50 (0.76)	131.0 (0.578)	0.195
El Reno, Oklahoma: EF19	35.557′N, 98.017′W	421	Pasture (ungrazed)	0.44 (0.69)	132.4 (0.515)	0.239
Meeker, Oklahoma: EF20	35.564′N, 96.988′W	309	Pasture	0.48 (0.70)	128.2 (0.554)	0.205

Mean and maximum values of NDVI are obtained from MODIS 16-day vegetation indices product obtained from April 2001 to May 2005. Mean soil moisture (SM, kg/kg) is obtained from surface soil moisture measurements taken at 2.5 cm, collected from April 2001 to May 2005. Mean evapotranspiration (ET, $W m^{-2}$) and evaporative fraction (EF) are also obtained from data collected from April 2001 to May 2005.

calculate sensible heat flux and ET using the Bowen ratio technique. The bulk aerodynamic technique is used to replace sunrise and sunset spikes in the flux data. The measurements and instruments are summarized in Table 2.

Net radiation (R_n) is measured at the EBBR sites using domed model $Q*6.1$ instruments manufactured by Radiation and Energy Balance Systems (REBS), mounted at the 2.6 m level. ET is estimated as a function of the Bowen ratio β:

$$\lambda E = \frac{R_n - G}{1+\beta} \tag{3}$$

where β is estimated from the vertical gradients of temperature (T_1, T_2) and specific humidity (q_1, q_2) at two heights in the following manner:

$$\beta = \frac{H}{\lambda E} = \frac{C_p K_h}{\lambda K_w}\frac{(T_1 - T_2)}{(q_1 - q_2)} \tag{4}$$

C_p is the isobaric specific heat for dry air and is equal to $1012 J kg^{-1} K^{-1}$, λ is the latent heat of vaporization, and K_h and K_w are the eddy diffusivities for heat and water vapor, respectively (Ohmura, 1982). The eddy diffusivities are assumed to be equal. Vertical gradients in air temperature and moisture are measured using temperature and humidity sensors mounted at heights of 2 and 3 m. An automatic exchange mechanism switches the two temperature and humidity sensors vertically every 15 min to minimize systematic errors due to instrument offset and drift. The average of data produced by two 13-min averages of 30-s samples yields a final 30-min mean of H and λE.

Table 2
Measurements and Instruments deployed at the South Great Plain Energy Balance Bowen Ratio (EBBR) sites

Net radiation only	$Q*6.1$
Ground heat flux	Five HFT3.1 ground flux plates installed at 5-cm depth Five REBS PRTDs installed at 0–5 cm depth, spaced 1.0 m apart
Sensible and latent heat fluxes	Bowen ration system: vertical temperature/moisture gradient measured between 2 and 3 m
Soil moisture	Five resistance-type SMP-2 sensors, installed at 2.5 cm depth, spaced 1.0 m apart

At each EBBR facility, soil heat flux G was estimated as the average of data from five soil heat plate sensors (the REBS HFT 3.1 s model) buried at a depth of 5 cm. The ground heat storage term was calculated as a function of the soil heat capacity (computed as a function of soil moisture and estimated at a depth of 2.5 cm) and the integrated soil temperature as observed from five soil heat plate sensors buried between 0 and 5 cm. The ARM EBBR facilities estimate the percent soil water (ratio of the mass of soil water to the mass of dry soil) from the soil water potential measured from five resistance-type soil moisture sensors (model SMP-2 manufactured by REBS). An average data value from the five soil heat plates and soil moisture sensors is used.

3. Variation and controlling factors of the evaporative fraction

We introduce "evaporative fraction (EF)" as an index for ET after Shuttleworth et al. (1989). EF is directly related to the Bowen ratio β:

$$\mathrm{EF} = \frac{\lambda E}{\lambda E + H} = \frac{\lambda E}{R_n - G} = \frac{1}{1+\beta} \tag{5}$$

However, we do not use β because: (1) β is a nonlinear parameter for ET, and (2) β does not have an upper limit (if ET approaches zero, β goes to infinity) (Nishida et al., 2003). In comparison, EF has the following advantages (Nishida et al., 2003): (1) EF is a suitable index for surface soil moisture condition, and (2) EF is useful for the temporal scaling.

To obtain the temporally averaged EF, the averaged ET and sensible heat flux is first calculated using the following relation:

$$\mathrm{EF} = \frac{\sum_{i-1}^{n} \lambda E_i}{\sum_{i=1}^{n} H_i + \sum_{i=1}^{n} \lambda E_i} \tag{6}$$

Table 3
The correlation coefficients between evaporative fraction (EF) and the midday air temperature ($r^2_{EF,tam}$), the daytime air temperature ($r^2_{EF,tad}$), NDVI ($r^2_{EF,NDVI}$), soil moisture ($r^2_{EF,SM}$) at 2.5 cm depth

Site	$r^2_{EF,tad}$	$r^2_{EF,tam}$	$r^2_{EF,NDVI}$	$r^2_{EFn,NDVI}$	$r^2_{EF,SM}$	$r^2_{EFn,SM}$	$r^2_{NDVI,SM}$
Ef02	0.515	0.489	0.001	0.197	−0.05	0.281	0.390
Ef04	0.405	0.360	0.000	0.062	0.086	0.295	0.254
Ef07	0.463	0.435	0.460	−0.093	−0.008	0.436	−0.335
Ef08	0.225	0.226	0.310	0.145	0.254	0.467	−0.084
Ef09	0.469	0.440	0.496	0.048	−0.065	0.098	0.080
Ef12	0.503	0.455	0.683	0.081	−0.224	0.119	−0.401
Ef13	0.500	0.460	−0.073	−0.075	−0.075	0.278	0.268
Ef15	0.574	0.545	0.433	0.0121	–	–	0.221
Ef18	0.559	0.518	0.567	0.063	−0.232	0.244	−0.491
Ef19	0.512	0.478	0.610	0.274	−0.222	0.229	−0.396
Ef20	0.388	0.3530	0.438	−0.059	0.115	0.410	−0.419

The correlation coefficients between normalized EF by air temperature controlling parameter $\Delta/(\Delta+\gamma)$ and NDVI ($r^2_{EFn,NDVI}$), and soil moisture ($r^2_{EFn,SM}$) are also shown, as are the correlation coefficients between NDVI and SM ($r^2_{NDVI,SM}$). The EF, the air temperature, the soil moisture are collected by the 11 enhanced facilities located throughout the Southern Great Plains from April 2001 to May 2005. The NDVI are from MODIS 16-day vegetation indices products from April 2001 to May 2005.

Temporally averaged EF can also be obtained by averaging EFs for each measurement of λE and H. The two averaging methods are similar because EF is apparently stability during daytime (Brutsaert & Sugita, 1992). However, the latter method is sensitive to the error of measurement of λE and H when their absolute values are low, such as measurements taken during early morning and late afternoon.

To identify factors that drive the variation of EF, data collected from April 2001 to May 2005 are analyzed at the 11 sites. Table 3 summarizes the correlation coefficients between EF and the air temperature, NDVI and soil moisture of the 11 sites. Fig. 2 gives an example of the time series of daytime EF, daytime average air temperature, NDVI and soil moisture at site EF12. Generally speaking, air temperature has the highest correlation with EF at all the sites. The variation of air temperature follows that of EF. The scatterplots of the EF as a function of the air temperature for 4 sites, shown in Fig. 3, demonstrates that EF increases linearly with air temperature. More importantly, the slopes are similar for the different sites. The scatter points show that there are some other factors influencing EF.

The following general form describing ET (Parlange & Albertson, 1995) illustrates this finding:

$$\lambda E = \psi\left[A\frac{\Delta}{\Delta+\gamma}(R_n - G) + B\frac{\gamma}{\Delta+\gamma}f(u)\left(e_a^* - e_a\right)\right] \quad (7)$$

where e_a is the air vapor pressure at a reference height (often 2 m), e_a^* is the air saturation vapor pressure, $\Delta = de^*/dT$ is the

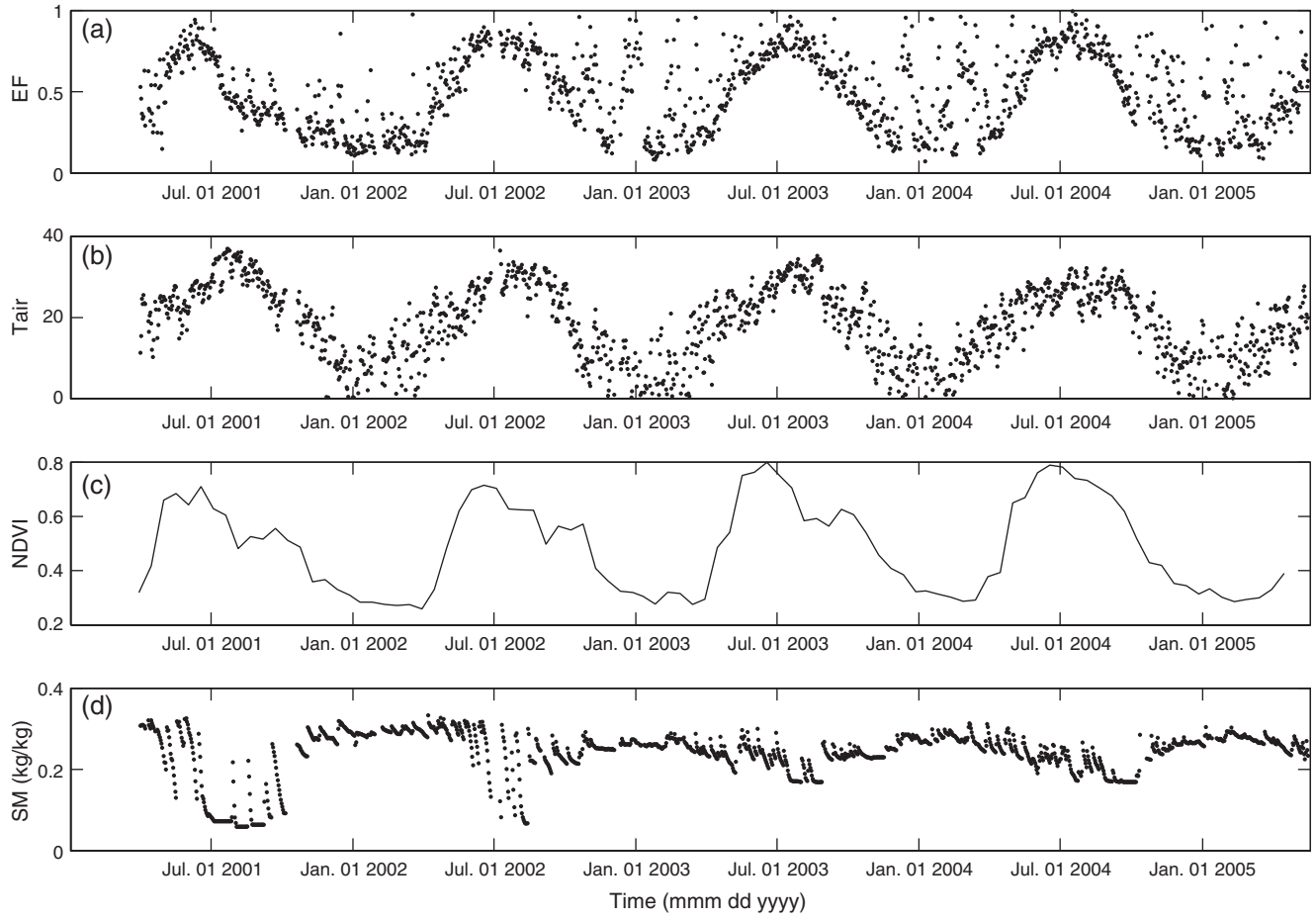

Fig. 2. An example the time serious of (a) the daily EF, (b) the daily air temperature, (c) the NDVI, and (d) the soil moisture (SM) at 2.5 cm depth during April 2001–May 2005 at sites EF12.

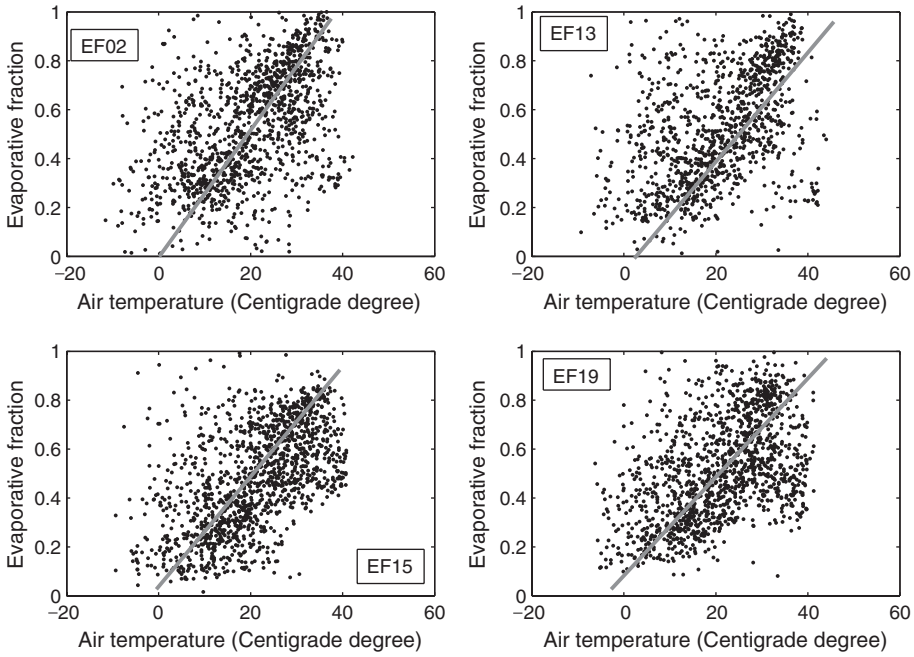

Fig. 3. The relationship between air temperature and evaporative fraction (EF) at sites of EF02, EF13, EF15 and EF19 using the data collected from April 2001 to May 2005. The correlation coefficients between EF and air temperature are shown in Table 3.

gradient of the saturated vapor pressure to the air temperature, and $\gamma = C_p/\lambda$ is the psychrometric constant. The $f(u)$ term represents some function of the wind velocity. A and B are model-dependent parameters, and Ψ is generally taken to be unity. The first term on the right-hand side of the equation represents the energy control on ET. The second term on the right-hand side of the equation represents the water vapor deficit control on ET, which is closely related to the water supply, soil evaporation and vegetation transpiration. When the water supply is sufficient, the available energy term dominates. Therefore, for water bodies and wet vegetation surfaces, Priestley and Taylor (1972) simplified Eq. (7) to:

$$\mathrm{EF} = \frac{\lambda E}{R_n - G} = \alpha \frac{\Delta}{\Delta + \gamma} \tag{8}$$

where $\alpha = 1.26$ is the so-called Priestley–Taylor parameter. Eichinger et al. (1996) analytically derived the Priestley–Taylor parameter α. They showed that it is equal to 1.26 for typically observed atmospheric conditions and is relatively insensitive to small changes in atmospheric parameters. For unsaturated soil (Komatsu, 2003) and vegetation surfaces where the water supply is limited (Davies & Allen, 1973), Eq. (8) becomes:

$$\mathrm{EF} = \alpha[(1 - \exp(-\theta/\theta_c)] \frac{\Delta}{\Delta + \gamma} \tag{9}$$

where θ is the surface soil moisture and θ_c is a parameter that depends on soil type and wind speed.

The term $\Delta/(\Delta+\gamma)$ in Eqs. (8) and (9) mainly depends on the air temperature:

$$\Delta = \frac{de^*}{dT} = \frac{0.622 \cdot \lambda \cdot e^*}{R_d \cdot T^2}, \tag{10}$$

Eq. (10) is the Clausius—Clapegron equation. To calculate simply, Richards (1971) suggested:

$$\Delta = \frac{373.15 \cdot e^*}{T_a^2} \cdot (13.3185 - 3.952 \cdot T_r - 1.9335 \cdot T_r^2 - 0.5196 \cdot T_r^3), \tag{11}$$

$$e^* = P_0 \cdot \exp(13.3185 \cdot T_r - 1.976 \cdot T_r^2 - 0.6445 \cdot T_r^3 - 0.1299 \cdot T_r^4), \tag{12}$$

$$T_r = 1 - 373.15/T_a \tag{13}$$

Psychrometric constant γ can be calculated from:

$$\gamma = \frac{C_p P}{0.622\lambda}, \tag{14}$$

$$P = P_0 \cdot 10^{\left(\frac{-z}{18\,400} \cdot \frac{T_a}{273}\right)}, \tag{15}$$

$$\lambda = 4.2 \times (597 - 0.6(T_a - 273)) \cdot 1000 \tag{16}$$

where T_a is the air temperature (K), z is the height above sea level (m), and $P_0 = 1013.15$ hPa is the standard atmospheric pressure at sea surface level. From Eqs. (11)–(16), one can see that the term $\Delta/(\Delta+\gamma)$ mainly depends on air temperature, therefore, $\Delta/(\Delta+\gamma)$ is referred to as the air temperature controlling factor. $\Delta/(\Delta+\gamma)$ is calculated using air temperatures varying from −10 °C to 40 °C and the average of the height above sea level of all the sites. Fig. 4 shows that the control parameter $\Delta/(\Delta+\gamma)$. increases nearly linearly with the air temperature. This is similar to the EF increasing nearly linearly with the air temperature as shown in Fig. 3. The slope of the relation shown in Fig. 4 is about 0.0127, which means that an

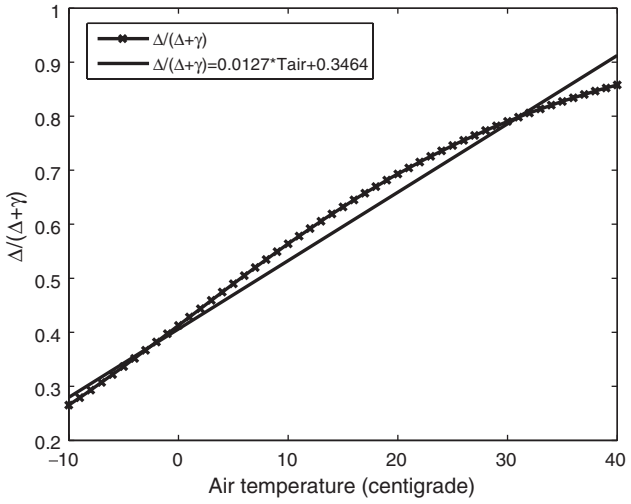

Fig. 4. Air temperature control factor $\Delta/(\Delta+\gamma)$ as a function of air temperature.

error in air temperature of 1 K will result in an error of 0.0127 α in Eq. (8).

Table 3 shows that the correlation coefficients between EF and soil moisture are very low, ranging in magnitude from 0.008 to 0.254. This does not mean that the influence of soil moisture on EF is negligible. Since the seasonal variation of soil moisture differ from that of EF and air temperature (see Fig. 2), low correlation coefficients are expected. Because the seasonal variation of air temperature is similar to that of EF, the air temperature control parameter is used to normalize the EF so that the seasonal variation is partly removed. The correlation coefficients between soil moisture and the normalized EF are noticeably improved, with magnitudes now ranging from 0.098 to 0.467. The largest correlations occur for the sites with the lowest soil moisture contents. This can be explained as follows. First, for sites with low soil moisture (such as site EF08, where the soil moisture is about 8% kg/kg) EF is mainly controlled by the water supply; when the water supply is sufficient, the energy term is dominant. Second, Kustas et al. (1993) showed that ET over a soil surface or sparse vegetation is mostly related to the soil moisture of the 0–5 cm layer; the soil moisture used here is measured at a depth of 2.5 cm. It was also found that ET of vegetation is closely related to the root zone soil moisture except in conditions of extreme soil water deficit (Arrett & Clark, 1994; Carlson et al., 1994).

The NDVI shows a similar seasonal variation with that of EF and the air temperature. Vegetation indices have been used as a main factor in estimating ET (Nagler et al., 2005a,2005b). Four sites (sites EF09, EF12, EF18 and EF19) with a high correlation between the NDVI and EF were selected to study more closely the relationship between the NDVI and EF. The results are illustrated in Fig. 5 which shows that there is a general increase in EF with the NDVI and that the slope varies from sites to site. This means that the influence of vegetation on EF depends on other parameters, such as soil moisture. The relationship between NDVI and EF is more scattered when NDVI is small, i.e. where the influence of soil moisture is dominant. Under these conditions, it is difficult to estimate EF from NDVI using a single empirical formula.

Furthermore, Table 3 shows that the correlation coefficients between the NDVI and the normalizing EF using the air temperature control parameter are very low, which shows that the air temperature control parameter in Eq. (8) can be used to parameterize EF well.

4. Estimating EF

The above analyses reveal that air temperature, NDVI and soil moisture are the three dominant factors influencing EF. It

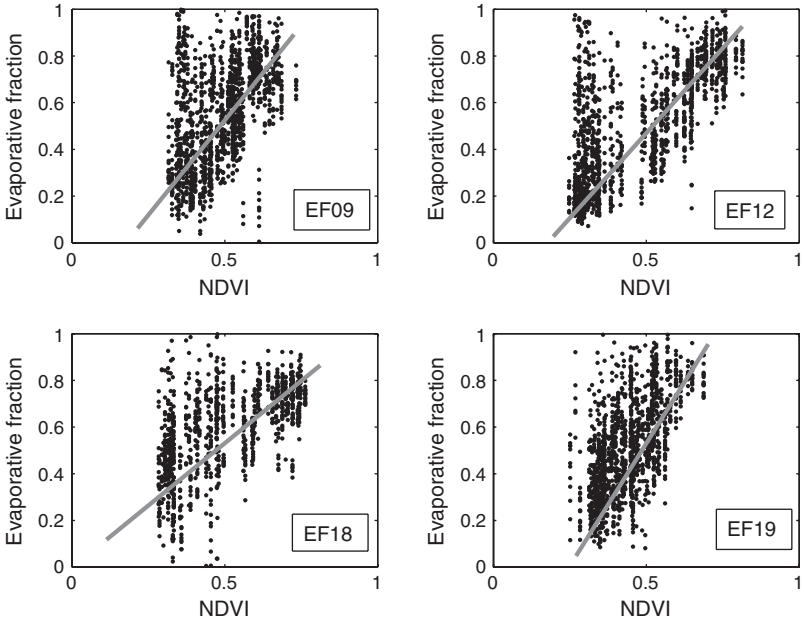

Fig. 5. The relationship between MODIS normalized difference vegetation index (NDVI) and evaporative fraction (EF) at sites EF09, EF12, EF18 and EF19 using the data collected from April 2001 to May 2005. The correlation coefficients between EF and NDVI are shown in Table 3.

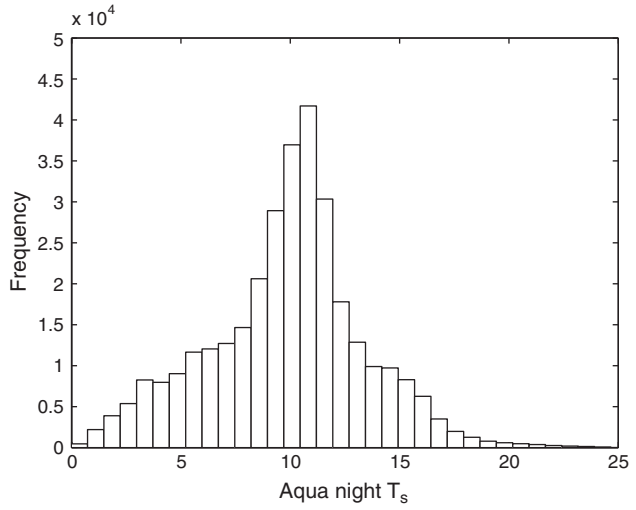

Fig. 6. A histogram of the nighttime T_s in the study region shown in Fig. 1 (about $550 \times 550\,km^2$) under clear sky conditions. The data was collected by Aqua at 1:45 AM on May 31 2004 (Julian day 152).

has been demonstrated that EF can be parameterized using the air temperature control parameter and the Priestley–Taylor parameter (Priestley & Taylor, 1972), which has been shown to depend on soil moisture content (Davies & Allen, 1973; Komatsu, 2002). Near surface air temperatures used in this paper are interpolated from NCEP (National Centers for Environment Prediction of U.S.) reanalysis near surface air temperature (at 2 m) data sets at a spatial resolution of $1° \times 1°$ and a temporal resolution of four times (at 0:00 AM, 6:00 AM, 12:00 PM, 6:00 PM, respectively, Universal Time) a day (http://dss.ucar.edu/datasets/ds083.2). These data sets supply reasonable estimation of near surface air temperature (Kalnay et al., 1996).

In the past, many investigators employed T_s–NDVI spatial variation to estimate soil moisture content or the Priestley–Taylor parameter. Sandholt et al. (2002) proposed one method to parameterize soil moisture based on the triangular distribution of T_s–NDVI. Wan et al. (2004a) used a similar method to estimate soil moisture content over SGP using MODIS land surface temperature and NDVI retrievals. Jiang and Islam (2001) directly estimated EF over SGP through the linear decomposition of the triangular distribution of the T_s–NDVI spatial variation.

The principle of these methods is simple: the temperature changes of wet surfaces are small since more energy is used for ET of wet surface and wet surface have higher thermal inertia (cooling effect). As such, the temperature used in these methods should be the temporal variation of T_s rather than T_s itself. However, in the previous investigations (Boegh et al., 1999; Jiang & Islam, 2001, 2003; Nishida et al., 2003; Venturini et al., 2004; Wan et al., 2004a), only the daytime retrievals of T_s over different locations were used rather than temporal variation of T_s, which resort to an implicit assumption that T_s at night is uniform across the study region. From the MODIS T_s retrievals during day and night, we can examine the day–night T_s difference, as well as the (ΔT_s–NDVI) spatial variation. Fig. 6 shows a histogram of nighttime T_s in the study region shown in Fig. 1 under clear sky conditions. Although the differences maybe result partially from retrieval artifacts, the variation of nighttime T_s is large enough that must be taken into account when using T_s–NDVI to estimate EF.

Fig. 7 gives examples of daytime T_s–NDVI spatial variations from Terra and Aqua measurements, differences between daytime Terra T_s and nighttime Aqua T_s as a function of NDVI, and differences between daytime Aqua T_s and nighttime Aqua T_s as a function of NDVI for a sample day. The overpass times for Aqua nighttime, Terra daytime and Aqua daytime measurements are about 2:00 AM, 11:20 AM and 1:10 PM, respectively, for the study region. One can see that the shapes of the T_s–NDVI spatial variations are similar to those of the T_s–NDVI spatial variations, making it possible to estimate the EF using a method similar to that using the T_s–NDVI spatial variation (Boegh et al., 1999; Prigent et al., 2005). Basically, the method extends the Priestley–Taylor parameter,α, by interpolating the parameter in a range of 0–1.26 according to NDVI and T_s over the study region and assuming that that the shape of the T_s–NDVI spatial variation is triangular (Jiang & Islam, 2001). The method is modified to the trapezoidal T_s–NDVI spatial variation (Jiang & Islam, 2003), which is tailored to include the day–night temperature difference (see Appendix A).

To examine the validity of using the day–night temperature difference and NDVI spatial variation (ΔT_s–NDVI), the EF retrieved using four combinations was compared: (1) Terra daytime T_s–NDVI, (2) Aqua daytime T_s–NDVI, (3) Terra daytime and Aqua nighttime temperature difference ΔT_s–NDVI, and (4) Aqua daytime and Aqua nighttime temperature difference T_s–NDVI. It should be noted that only the difference between Aqua and Terra daytime T_s lies in the measurement time, i.e. about 10:30 AM for Terra daytime and about 1:30 PM for Aqua. The validations were carried out for sixteen days during 2004. They are Julian days (day number of a year) 105, 126, 127, 128, 129,143, 144, 152, 163, 230, 242, 252, 257, 260, 262, and 277, covering a period from April to October. The sites shown in Fig. 1 were used to validate the MODIS-retrieved EF. The year 2004 is selected because all the required satellite and ground-based measurements are available during this period. These days are selected because they are clear days for all the validation sites shown in Table 1. The retrievals of MODIS-based EF are averaged over four pixels enclosing the ground-based site.

Fig. 8 shows the comparison between the MODIS-retrievals and the corresponding ground-based measurements. One can see that the ΔT_s–NDVI EF retrievals improve distinctly in comparison with those retrieved from the daytime temperature. Note that the scatter points in the comparison stems partially from incompatibility due to different spatial scales of the data and the heterogeneity of the surface. For the heterogeneous surface, the scale of ground-based measurement of EF depends on the fetch length which depends on wind speed and wind direction, while MODIS EF retrievals have a scale of 1 km.

Table 4 presents the biases (BIAS), mean deviations (MD), standard deviations (S.D.), and correlation coefficients of the relationships illustrated in Fig. 8. The Aqua daytime EF

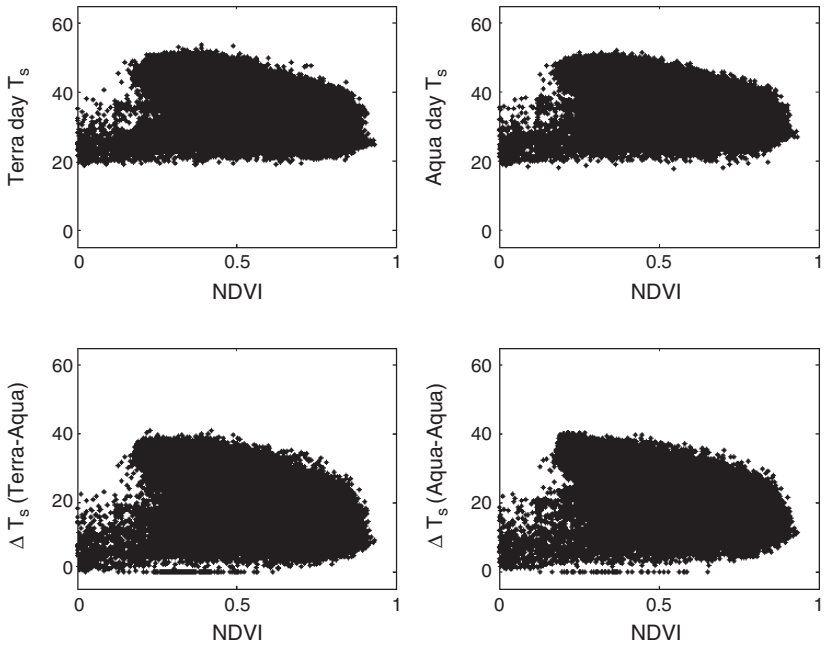

Fig. 7. Examples of spatial variations of the daytime T_s–NDVI of the Aqua and Terra, the difference of T_s of daytime Terra and nighttime Aqua night and NDVI (T_s–NDVI,Terra–Aqua), the difference of T_s of daytime Aqua and nighttime Aqua (ΔT_s–NDVI,Terra–Aqua). The data were collected at May 6, 2004 (Julian day 127).

retrievals are better than those from the Terra daytime, and Aqua daytime and aqua nighttime difference retrievals are better than those from Terra daytime and Aqua nighttime difference. Venturini et al. (2004) argued that that EF retrieval is not sensitive to satellite overpass time, which is seen in Table 4 in terms of the bias. However, the values of the correlation coefficient, standard deviation and mean deviation suggest that Aqua retrieval is better than those of Terra retrievals. Table 4 shows that the mean difference for all the sites (mean of the absolute value of difference between ground-based measurements and EF retrievals) is 0.106. Considering the mean value of the EF is 0.6, one can estimate that the relative error is 17%.

Table 4 also shows that, in terms of the correlation coefficient, sites EF02, EF07, EF09, EF12, EF13, EF18, EF19 and EF20 are reasonably good, but sites EF04, EF08 and EF15 are not so good. This may be explained by the

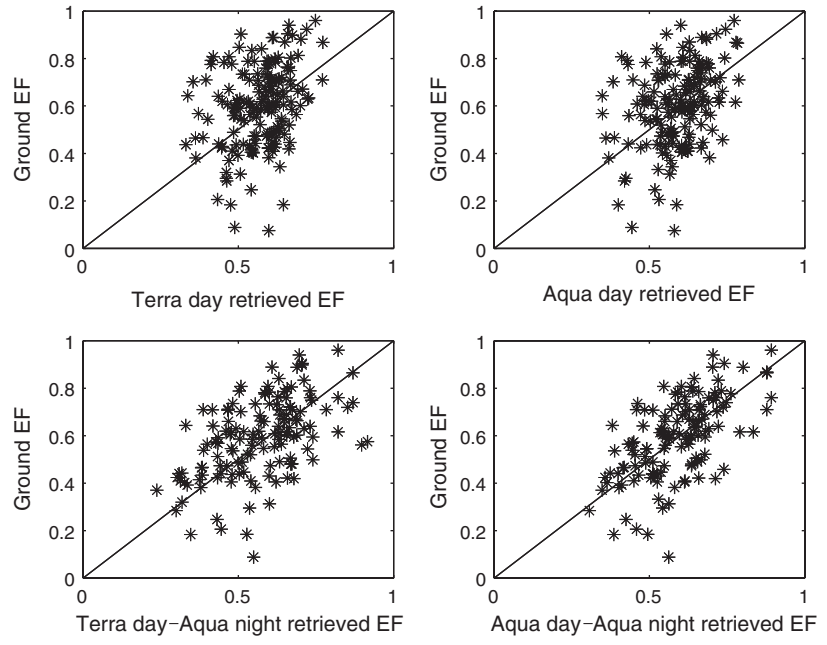

Fig. 8. Ground-based measurements of the EF as a function of the corresponding MODIS retrievals from four spatial variations: daytime T_s–NDVI of Aqua and Terra, the difference of T_s of daytime Terra and nighttime Aqua night and NDVI (ΔT_s–NDVI,Terra–Aqua), the difference of T_s of daytime Aqua and nighttime Aqua (ΔT_s–NDVI,Terra–Aqua). The statistics parameters are shown in the last four lines of Table 4.

heterogeneity of the EF. Chen and Brusaert (1995) showed that the spatial distribution of ET is strongly related to the distribution of soil moisture and of the state of the vegetation. The strength of these relationships depends on soil moisture content and its spatial distribution. When the mean soil content is high, the distribution of evaporation is quite uniform regardless of the vegetation uniformity. In the intermediate range, both soil moisture and vegetation contribute to the spatial distribution. When soil moisture is low, it is normally non-uniform, and spatial distribution of soil moisture becomes the primary control of the spatial variation of EF. For the sites having better correlation, their soil moisture is high – about 20% (kg/kg) (cf. Table 1), whereas sites EF04 and EF08 have much low soil moisture content – about 8% (kg/kg). EF15 lies in region of varying land cover type (see Fig. 1).

Table 4
The statistical parameters of the difference of the MODIS EF retrievals and the ground-based measurements: bias (BIAS), mean deviation (MD), standard deviation (S.D.), and correlate coefficient (R^2) from four combinations: (1) Terra daytime T_s–NDVI, (2) Aqua daytime T_s–NDVI, (3) Terra daytime and Aqua nighttime difference ΔT_s–NDVI (Terra day–Aqua night), (4) Aqua daytime and Aqua nighttime difference ΔT_s–NDVI (Aqua day–Aqua night)

Site	Method	BIAS	MD	S.D.	R^2
EF02	Terra day	−0.182	0.214	0.148	−0.124
	Aqua day	−0.142	0.166	0.142	0.057
	Terra day–Aqua night	−0.142	0.191	0.168	0.142
	Aqua day–Aqua night	−0.106	0.123	0.12	0.466
EF04	Terra day	0.089	0.134	0.157	−0.027
	Aqua day	0.097	0.119	0.13	0.14
	Terra day–Aqua night	0.106	0.132	0.131	0.48
	Aqua day–Aqua night	0.131	0.138	0.12	0.431
EF07	Terra day	−0.091	0.155	0.148	0.518
	Aqua day	−0.065	0.143	0.152	0.428
	Terra day–Aqua night	−0.076	0.138	0.154	0.554
	Aqua day–Aqua night	−0.04	0.114	0.14	0.645
EF08	Terra day	−0.01	0.173	0.202	−0.124
	Aqua day	0.002	0.174	0.207	−0.369
	Terra day–Aqua night	0.003	0.173	0.207	0.004
	Aqua day–Aqua night	0.013	0.143	0.176	0.159
EF09	Terra day	−0.069	0.101	0.112	0.387
	Aqua day	−0.031	0.093	0.116	0.301
	Terra day–Aqua night	−0.052	0.067	0.077	0.784
	Aqua day–Aqua night	−0.01	0.069	0.088	0.697
EF12	Terra day	0.042	0.134	0.164	0.365
	Aqua day	0.068	0.138	0.154	0.452
	Terra day–Aqua night	0.092	0.146	0.153	0.605
	Aqua day–Aqua night	0.08	0.112	0.116	0.77
EF13	Terra day	−0.012	0.118	0.147	0.689
	Aqua day	0.005	0.099	0.133	0.73
	Terra day–Aqua night	0.008	0.109	0.144	0.68
	Aqua day–Aqua night	0.011	0.072	0.098	0.89
EF15	Terra day	0.067	0.176	0.228	−0.468
	Aqua day	0.07	0.198	0.244	−0.634
	Terra day–Aqua night	0.004	0.137	0.166	0.039
	Aqua day–Aqua night	0.013	0.14	0.161	−0.081
EF18	Terra day	−0.051	0.125	0.138	0.07
	Aqua day	−0.022	0.112	0.131	0.164
	Terra day–Aqua night	−0.05	0.096	0.1	0.703
	Aqua day–Aqua night	−0.014	0.084	0.108	0.688
EF19	Terra day	0.032	0.122	0.155	−0.413
	Aqua day	0.05	0.128	0.155	−0.312
	Terra day–Aqua night	−0.016	0.06	0.084	0.668
	Aqua day–Aqua night	0.018	0.072	0.108	0.382
EF20	Terra day	−0.022	0.112	0.14	0.063
	Aqua day	−0.005	0.121	0.154	−0.095
	Terra day–Aqua night	−0.019	0.105	0.131	0.493
	Aqua day–Aqua night	0.013	0.088	0.102	0.643
Total	Terra day	−0.033	0.141	0.171	0.286
	Aqua day	−0.014	0.134	0.166	0.34
	Terra day–Aqua night	−0.022	0.124	0.153	0.515
	Aqua day–Aqua night	−0.002	0.106	0.136	0.605

Notes to Table 4
The average of the ground EF measurements is 0.6 for all the comparison days and sites used here.
Bias (BIAS), mean deviation (MD), standard deviation (S.D.) are defined as:

$$\mathrm{MD} = \frac{1}{n}\sum_{i=1}^{n} \mathrm{abs}(\mathrm{EF}_{\mathrm{dif,i}})$$

$$\mathrm{S.D.} = \sqrt{\frac{1}{n}\sum_{i=1}^{n} (\mathrm{EF}_{\mathrm{dif,i}} - \mathrm{BIAS})^2}$$

$$\mathrm{BIAS} = \frac{1}{n}\sum_{i=1}^{n} \mathrm{EF}_{\mathrm{dif,i}}$$

$$\mathrm{EF}_{\mathrm{dif,i}} = \mathrm{EF}_{\mathrm{MODIS,\ i}} - \mathrm{EF}_{\mathrm{ground,i}}$$

where n is the sample number.

5. Conclusions

Satellite remote sensing is one promising technique to estimate global or regional ET or EF. However, current methods using the gradient between T_s and near surface air temperature to estimate ET (or EF) are sensitive to the retrieval errors of T_s and the interpolation errors of air temperature from the ground-based point measurements. Two methods have been proposed to reduce this sensitivity: the thermal inertia method and the T_s–NDVI spatial variation method. The former uses the temporal difference between T_s retrievals, and the latter uses the spatial information of T_s. A different approach is proposed in this study that employs day–night T_s difference–NDVI(ΔT_s–NDVI) which use the temporal and spatial information of T_s, following the parameterization proposed by Jiang and Islam (2001) which used the daytime T_s only.

Taking advantage of satellite measurements and the extensive ground-based measurements available at the 11 enhanced surface facility sites throughout the Great South Plain from April 2001 to May 2005, EF was analyzed in order to obtain a proper parameterization of EF. The dominant factors driving the seasonal variation of EF are air temperature and normalized difference vegetation index. Data analyses show that the EF can be parameterized as a function of the air temperature controlling parameter $\Delta/(\Delta+\gamma)$ and the Priestley–Taylor parameter, α, which depends on soil moisture contents. Soil moisture content and EF are poorly correlated but the correlation improves considerably after the seasonal trend of EF is removed. Therefore, soil moisture is also one important factor influencing EF, which is extracted from the spatial variation of a newly proposed method using ΔT_s–NDVI.

Following the approach of Jiang and Islam (2001), we propose to use the ΔT_s difference in lieu of the daytime T_s. Yet, the method was modified to be applicable to both the triangular

or trapezoidal shapes for ΔT_s–NDVI domain. Improvement in the accuracy of EF retrievals was shown by applying the revised ΔT_s–NDVI and the original ΔT_s–NDVI methods to the same ground-based measurements. The retrievals of the EF are improved in terms of bias error, mean deviation, standard deviation, and correlation coefficient. The accuracy of the EF retrieval is on the order of 17%, which is considered satisfactory, given the simplicity of the new method and the number of input variables of the method. While some approaches may achieve higher accuracies, they often either require additional information obtained by in situ measurements, or the calibration of their methods against ground observations.

When the EF is ready, it can be easily used to partition the surface net radiation budget. Satellite remote sensed data have been use to estimate global net radiation and the accuracy improves thanks to numerous techniques proposed with proven high accuracy (for example, Allan et al., 2004; Bisht et al., 2005; Diak et al., 2004; Gupta et al., 1999; Li & Leighton, 1993; Li et al., 2005; Wang et al., 2005b,2005c; Zhang et al., 2004).

Acknowledgments

We would like to thank the two anonymous reviewers for their critical and helpful comments and suggestions. This research was jointly funded by US Department of Energy's Atmospheric Radiation Program with a grant DEF-G0201ER63166 and the National Science Foundation of China (40520120071) and an opening funding of the national Key Laboratory for Remote Sensing Science (SK050012). We also thank to Dr. Michael Sparrow from the International CLIVAR Project Office for helpful comments.

Appendix A. Derivation of the modified ΔT_s–NDVI for estimating EF

Fig. A1 shows the schematic plot for the interpretation of the Priestley–Taylor parameter, α. The trapezoid ABCD represents the T_s–NDVI or ΔT_s–NDVI spatial variation; CD is the "cold edge" and AB is the "warm edge" of the spatial variation. Three assumptions made by Jiang and Islam (2001) were adopted here: (1) the cold edge has the maximum $\alpha_{max}=1.26$ (for example, α at points F and G of Fig. A1 is both equal to 1.26), (2) the maximum temperature of the warm edge has minimum $\alpha_{max}=0.0$ (point A in Fig. A1), and (3) the relationship between α and the spatial variation of T_s (or ΔT_s) is linear. The linear interpolation of T_s–NDVI is adopted by Jiang and Islam (2001) to parameterize α. Sandholt et al. (2002) and Wan et al. (2004a) estimated the soil water index by linearly interpolating the T_s–NDVI spatial variation. For pixel i at E(T_s–NDVI), connect A and E, and extend AE to G. Because α at point A is equal to α_{min} and "cold edge" has the maximum α_{max}, the length of AG is $\alpha_{max}-\alpha_{min}$, and the length of AE is $\alpha_i-\alpha_{min}$. Because the triangle EFG is similar to triangle ACG, the following equation can be derived:

$$\frac{|EF|}{|AC|}=\frac{|EG|}{|AG|} \tag{A1}$$

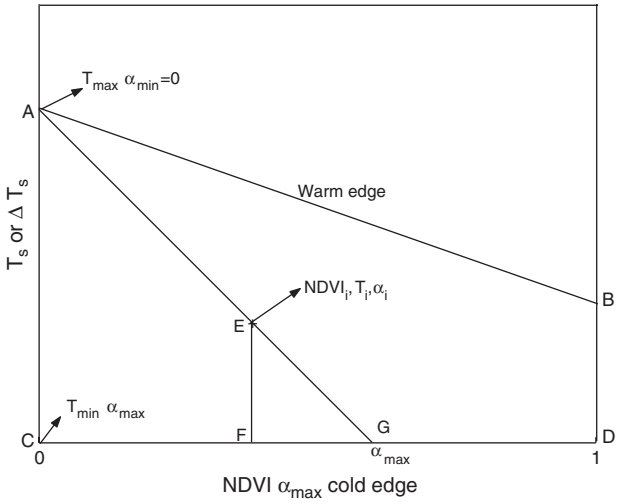

Fig. A1. A schematic plot interpretating the Priestly–Taylor parameter, α.

Eq. (A1) can be written as:

$$\frac{T_i-T_{min}}{T_{max}-T_{min}}=\frac{(\alpha_{max}-\alpha_{min})-(\alpha_i-\alpha_{min})}{\alpha_{max}-\alpha_{min}} \tag{A2}$$

α_i at (T_i,NDVI) is equal to:

$$\alpha_i=\frac{T_{max}-T_i}{T_{max}-T_{min}}(\alpha_{max}-\alpha_{min})+\alpha_{min} \tag{A3}$$

where T is the T_s in the T_s–NDVI or (ΔT_s in the ΔT_s–NDVI) spatial variation. T_{max} and T_{min} are determined from the spatial variations as shown in Fig. 7, α_{max} and α_{min} is same as that used in Jiang and Islam (2001).

The EF retrieved using the above parameterization is the same as that of Jiang and Islam (2001). However, the method proposed here is more direct, and is more easily used in other situations, such as parameterization of EF in model simulation with the satellite remote sensed land surface temperature.

Therefore, EF is parameterized as:

$$EF=\frac{\Delta}{\Delta+\gamma}\left[\frac{T_{max}-T_i}{T_{max}-T_{min}}(\alpha_{max}-\alpha_{min})+\alpha_{min}\right] \tag{A4}$$

The sensitivity of EF to T_{max}, T_{min}, α_{max}, α_{min} can be written as:

$$\frac{\partial EF}{\partial T_{max}}=\frac{\Delta}{\Delta+\gamma}(\alpha_{max}-\alpha_{min})\frac{T_i-T_{min}}{(T_{max}-T_{min})^2} \tag{A5}$$

$$\frac{\partial EF}{\partial T_{min}}\frac{\Delta}{(\Delta+\gamma)}(\alpha_{max}-\alpha_{min})\frac{T_{max}-T_i}{(T_{max}-T_{min})^2} \tag{A6}$$

$$\frac{\partial EF}{\partial \alpha_{max}}=\frac{\Delta}{\Delta+\gamma}\frac{T_{max}-T_i}{T_{max}-T_{min}} \tag{A7}$$

and

$$\frac{\partial EF}{\partial \alpha_{min}}=1-\frac{\Delta}{\Delta+\gamma}\frac{T_{max}-T_i}{T_{max}-T_{min}}=1-\frac{\partial EF}{\partial \alpha_{max}} \tag{A8}$$

From Eqs. (A5) (A6), one can estimate that $\partial EF/\partial T_{max}$ and $\partial EF/\partial T_{min}$ both have a typical value of about 0.02. Therefore, the sensitivity of EF to T_{max} and T_{min} is relative low. Using the slope of $\Delta/(\Delta+\gamma)$ to air temperature T_{air} (see Section 3), the sensitivity of EF to air temperature can be written as:

$$\frac{\partial EF}{\partial T_{air}} = 0.0127\left[\frac{T_{max}-T_i}{T_{max}-T_{min}}(\alpha_{max}-\alpha_{min})+\alpha_{min}\right]. \quad (A9)$$

References

Albellaoui, A., Becker, F., & Olory-hechinger, E. (1986). Use of Metesat for mapping thermal inertia and evapotranspiration over a limited region of Mali. *Journal of Climate and Applied Meteorology*, *25*, 1489–1506.

Allan, R. P., Ringer, M. A., Pamment, J. A., & Slingo, A. (2004). Simulation of the Earth's radiation budget by the European Centre for Medium-Range Weather Forecasts 40-year reanalysis (ERA40). *Journal of Geophysical Research*, *109*, D18107. doi:10.1029/2004JD004816.

Anderson, M. C., Norman, J. M., Diak, G. R., Kustas, W. P., & Mecikalski, J. R. (1997). A two-source time-integrated model for estimating surface flux using thermal infrared remote sensing. *Remote Sensing of Environment*, *60*, 195–216.

Arrett, R. W., & Clark, C. A. (1994). Functional relationship among soil moisture, vegetation cover and surface fluxes. In: *Proceedings 21st Conference in Agricultural and Forest Meteorology. American Meteorological Society, March 7–11, San Diego, CA*, J37–J38.

Baldocchi, D., Falge, E., Gu, L., Olson, R., Hollinger, D., Running, S., et al. (2001). Fluxnet: A new tool to study the temporal and spatial variability of ecosystem-scale carbon dioxide, water vapor, and energy flux densities. *Bulletin of the American Meteorological Society*, *82*(11), 2415–2434.

Bisht, G., Venturini, V., Islam, S., & Jiang, L. (2005). Estimation of the net radiation using MODIS (moderate resolution imaging spectroradiometer) data for clear sky days. *Remote Sensing of Environment*, *97*, 52–67.

Boegh, E., Soegaard, H., Hanan, N., Kabat, P., & Lesch, L. (1999). A remote sensing study of the NDVI–T_s relationship and the transpiration from sparse vegetation in the Sahel based on high-resolution satellite data. *Remote Sensing of Environment*, *69*, 224–240.

Brotzge, J. A., & Kenneth, C. C. (2003). Examination of the surface energy budget: A comparison of eddy correlation and Bowen ratio measurement systems. *Journal of Hydrometeorology*, *4*(2), 160–178.

Brutsaert, W., & Sugita, M. (1992). Application of self-preservation in the diurnal evolution of the surface energy budget to determine daily evaporation. *Journal of Geophysical Research*, *97*(D17), 18377–18382.

Caparrini, F., Castelli, F., & Entekhabi, D. (2004). Estimating of surface turbulent fluxes through assimilation of radiometric surface temperature sequences. *Journal of Hydrometeorology*, *5*, 145–159.

Carlson, T. N., Gillies, R. R., & Perry, E. M. (1994). A method to make use of thermal infrared temperature and NDVI measurements to infer surface soil water content and fractional vegetation cover. *Remote Sensing Reviews*, *9*, 161–173.

Carlson, T. N., Gillies, R. R., & Schmugge, T. J. (1995). An interpretation of methodologies for indirect measurement of soil water content. *Agricultural and Forest Meteorology*, *77*, 191–205.

Chen, D., & Brusaert, W. (1995). Diagnostics of land surface spatial variability and water vapor flux. *Journal of Geophysical Research*, *100*(D12), 25,595–25,606.

Coll, C., Caselles, V., Galve, J. M., Valor, E., Niclos, R., Sanchez, J. M., et al. (2005). Ground measurements for the validation of land surface temperatures derived from AATSR and MODIS data. *Remote Sensing of Environment*, *97*, 288–300.

Davies, J. A., & Allen, C. D. (1973). Equilibrium, potential and actual evaporation from cropped surface in southern Ontario. *Journal of Applied Meteorology*, *12*, 649–657.

Diak, G. R., Mecikalski, J. R., Anderson, M. C., Norman, J. M., Kustas, W. P., Torn, R. D., et al. (2004). Estimating land surface energy budgets from space: Review and current efforts at the University of Wisconsin—Madison and USDA–ARS. *Bulletin of the American Meteorological Society*, *85*(1), 65–78.

Eichinger, W. E., Parlange, M. B., & Stricker, H. (1996). On the concept of equilibrium evaporation and the value of the Priestley–Taylor coefficient. *Water Resource Research*, *32*(1), 161–164.

Friedl, M. A. (2002). Forward and inverse modeling of land surface energy balance using surface temperature measurements. *Remote Sensing of Environment*, *79*, 344–354.

Friedl, M. A., & Davis, F. W. (1994). Sources of variation in radiometric surface temperature over a tallgrass prairie. *Remote Sensing of Environment*, *48*, 1–17.

Gillies, R. R., Carlson, T. N., Cui, J., Kustas, W. P., & Humes, K. S. (1997). A verification of the 'triangle' method for obtaining surface soil water content and energy fluxes from remote measurements of the normalized difference vegetation index (NDVI) and surface radiant temperature. *International Journal of Remote Sensing*, *18*(15), 3145–3166.

Gómeza, M., Olioso, A., Sobrinoa, J. A., & Jacob, F. (2005). Retrieval of evapotranspiration over the Alpilles/ReSeDA experimental site using airborne POLDER sensor and a thermal camera. *Remote Sensing of Environment*, *96*, 399–408.

Goward, S. N., Xue, Y., & Czajkowski, K. P. (2002). Evaluating land surface moisture conditions from the remotely sensed temperature/vegetation index measurements. An exploration with the simplified simple biosphere model. *Remote Sensing of Environment*, *79*, 225–242.

Gupta, S. K., Ritchey, N. A., Wilber, A. C., Whitlock, C. H., Gibson, G. G., & Stackhous Jr., P. W. (1999). A climatology of surface radiation budget derived from satellite data. *Journal of Climate*, *12*, 2691–2710.

Huete, A., Didan, K., Miura, T., Rodriguez, E. P., Gao, X., & Ferreira, L. G. (2002). Overview of the radiometric and biophysical performance of the MODIS vegetation indices. *Remote Sensing of Environment*, *83*, 195–213.

Jiang, L., & Islam, S. (2001). Estimation of surface evaporation map over Southern Great Plains using remote sensing data. *Water Resources Research*, *37*(2), 329–340.

Jiang, L., & Islam, S. (2003). An intercomparison of regional latent heat flux estimation using remote sensing data. *International Journal of Remote Sensing*, *24*(11), 2221–2236.

Kalnay, E., Kanamitsu, M., Kistler, R., Collons, W., Deaven, D., Gandin, L., et al. (1996). The NCEP/NCAR 40-year reanalysis project. *Bulletin of the American Meteorological Society*, *77*(3), 437–471.

Komatsu, T. S. (2003). Toward a robust phenomenological expression of evaporation efficiency for unsaturated soil surface. *Journal of Applied Meteorology*, *42*, 1330–1334.

Kustas, W., Choudhury, B., Reginato, M. M. R., Jackson, R., Gay, L., & Weaver, H. (1989). Determination of sensible heat flux over sparse canopy using thermal infrared data. *Agricultural and Forest Meteorology*, *44*, 197–216.

Kustas, W. P., Schmugge, T. J., Humes, K. S., Jackson, T. J., Party, R., Weltz, M. A., et al. (1993). Relationship between evaporative fraction and remotely sensed vegetation index and microwave brightness temperature for semiarid rangelands. *Journal of Applied Meteorology*, *32*, 1781–1790.

Li, Z., Cribb, M., Chang, F. -L., Trishchenko, A., & Yi, L. (2005). Natural variability and sampling errors in solar radiation measurements for model validation over the ARM/SGP region. *Journal of Geophysical Research*, *110*, D15S19. doi:10.1029/2004JD005028.

Li, Z., & Leighton, H. G. (1993). Global climatologies of solar radiation budgets at the surface and in the atmosphere from 5 years of ERBE data. *Journal of Geophysical Research*, *98*, 4919–4930.

Monin, A. S., & Oblukhov, A. M. (1954). Basic laws of turbulent mixing in the atmosphere near the ground. *Trudy Geofizicheskogo Instituta Akademiya Nuak SSSR*, *24*(151), 163–187.

Monteith, J. L. (1973). *Principles of environmental physics.* Edward Arnold Press. 241 pp.

Moran, M. S., Clarke, T. R., Inoue, Y., & Vidal, A. (1994). Estimating crop water deficit using the relation between surface–air temperature and spectral vegetation index. *Remote Sensing of Environment*, *49*, 246–263.

Nagler, P. L., Cleverly, J., Glenn, E., Lampkin, D., Huete, A., & Wan, Z. (2005a). Predicting riparian evapotranspiration from MODIS vegetation indices and meteorological data. *Remote Sensing of Environment*, *94*(1), 17–30.

Nagler, P. L., Scott, R. L., Westenburg, C., Cleverly, J. R., Glenn, E. P., & Huete, A. R. (2005b). Evapotranspiration on western US rivers estimated using the enhanced vegetation index from MODIS and data from eddy covariance and Bowen ratio flux towers. *Remote Sensing of Environment*, *97*(3), 337–351.

Nemani, R. R., & Running, S. W. (1989). Estimation of regional surface resistance to evapotranspiration from NDVI and thermal-IR AVHRR data. *Journal of Applied Meteorology*, *28*, 276–284.

Nishida, K., Nemani, R. R., Running, S. W., & Glassy, J. M. (20034270). An operational remote sensing algorithm of land surface evaporation. *Journal of Geophysical Research*, *108*(D9). doi:10.1029/2002JD002062.

Norman, J. M., Kustas, W. P., Prueger, J. H., & Diak, G. R. (2000). Surface flux estimation using radiometric temperature: A dual temperature-difference method to minimize measurement errors. *Water Resource Research*, *36*(8), 2263–2274.

Ohmura, A. (1982). Objective criteria for rejecting data for Bowen ratio flux calculations. *Journal of Applied Meteorology*, *21*, 595–598.

Parlange, M. B., & Albertson, J. D. (1995). Regional scale evaporation and the atmospheric boundary layer. *Reviews of Geophysics*, *33*(1), 99–124.

Prata, A. J., & Cechet, R. P. (1999). An assessment of the accuracy of land surface temperature determination from the GMS-5 VISSR. *Remote Sensing of Environment*, *67*, 1–14.

Pratt, A. A., & Ellyett, C. D. (1979). The thermal inertia approach to mapping of soil moisture and geology. *Remote Sensing of Environment*, *8*, 151–168.

Price, J. C. (1977). Thermal inertia mapping: A new view of the Earth. *Journal of Geophysical Research*, *82*, 2582–2590.

Price, J. C. (1982). On the use of satellite data to infer surface fluxes at meteorological scales. *Journal of Applied Meteorology*, *21*, 1111–1122.

Price, J. C. (1990). Using spatial context in satellite data to infer regional scale evapotranspiration. *IEEE Transactions on Geoscience and Remote Sensing*, *28*, 940–948.

Priestley, C. H. B., & Taylor, R. J. (1972). On the assessment of surface heat flux and evaporation using large-scale parameters. *Monthly Weather Review*, *100*, 81–92.

Prigent, C., Aires, F., Rossow, W. B., & d Robock, A. (2005). Sensitivity of satellite microwave and infrared observations to soil moisture at a global scale: Relationship of satellite observations to in situ soil moisture measurements. *Journal of Geophysical Research*, *110*(D07110). doi:10.1029/2004JD005087.

Richards, J. M. (1971). Simple expression for the saturation vapor pressure of water in the range −50° to 140°. *British Journal of Applied Physics*, *4*, 115–118.

Roerink, G. J., Su, Z., & Menenti, M. (2000). S-SEBI: A simple remote sensing algorithm to estimate the surface energy balance. *Physics and Chemistry of the Earth. Part B: Hydrology, Oceans and Atmosphere*, *25*(2), 147–157.

Rowntree, P. R. (1991). Atmospheric parameterization for evaporation over land: Basic concept and climate modeling aspects. In T. J. Schmugge, & J. C. André (Eds.), *Land surface evaporation fluxes: Their measurements and parameterization* (pp. 5–30). New York: Springer-Verlag.

Salomonson, V., Barnes, W., Maymon, P., Montgomery, H., & Ostrow, H. (1989). MODIS: Advanced facility instrument for studies of the Earth as a system. *IEEE Transactions on Geoscience and Remote Sensing*, *27*, 145–153.

Sandholt, I., Ramussen, K., & Anderson, J. (2002). A simple interpretation of surface temperature/vegetation index space for assessment of surface moisture status. *Remote Sensing of Environment*, *79*, 213–224.

Shuttleworth, W. J., Gurney, R. J., Hsu, A. Y., & Ormsby, J. P. (1989). FIFE: The variation in energy partition at surface flux sites. In A. Rango (Ed.), *Remote sensing and large-scale processes* (Proceedings of the IAHS third international Assembly, Baltimore, MD, May, 1989). IAHS Publication, vol. 186. (pp. 67–74).

Smith, R. C. G., & Choudhury, B. J. (1991). Analysis of normalized difference and surface temperature observations over southeastern Australia. *International Journal of Remote Sensing*, *12*(10), 2021–2044.

Sobrino, J. A., & EL Kharraz, M. H. (1999). Combing afternoon and morning NOAA satellites for thermal inertia estimation: 2. Methodology and application. *Journal of Geophysical Research*, *104*(D8), 9455–9465.

Su, Z., Pelgrum, H., & Menenti, M. (1999). Aggregation effects of surface heterogeneity in land surface processes. *Hydrology and Earth System Sciences*, *3*(4), 549–563.

Venturini, V., Bisht, G., Islam, S., & Jiang, L. (2004). Comparison of EFs estimated from AVHRR and MODIS sensors over South Florida. *Remote Sensing of Environment*, *93*, 77–86.

Verstraeten, W. W., Veroustraete, F., & Feyen, J. (2005). Estimating evapotranspiration of European forests from NOAA-imagery at satellite overpass time: Towards an operational processing chain for integrated optical and thermal sensor data products. *Remote Sensing of Environment*, *96*, 256–276.

Wan, Z., & Dozier, J. (1996). A generalized split-window algorithm for retrieving land-surface temperature from space. *IEEE Transactions on Geoscience and Remote Sensing*, *34*(4), 892–905.

Wan, Z., & Li, Z. -L. (1997). A physics-based algorithm for retrieving land-surface emissivity and temperature from EOS/MODIS data. *IEEE Transactions on Geoscience and Remote Sensing*, *35*(4), 980–996.

Wan, Z., Wang, P., & Li, X. (2004a). Using MODIS land surface temperature and normalized difference vegetation index products for monitoring drought in the Southern Great Plains, USA. *International Journal of Remote Sensing*, *25*(1), 61–72.

Wan, Z., Zhang, Y. -L., Zhang, Q. -C., & Li, Z. -L. (2002). Validation of the land surface temperature products retrieved from terra moderate resolution imaging spectroradiometer data. *Remote Sensing of Environment*, *83*, 163–180.

Wan, Z., Zhang, Y. -L., Zhang, Q. -C., & Li, Z. -L. (2004b). Quality assessment and validation of the MODIS global land surface temperature. *International Journal of Remote Sensing*, *25*(1), 261–274.

Wang, K., Liu, J., Wan, Z., Wang, P., Michael, S., & Haginoya, S. (2005a). Preliminary accuracy assessment of MODIS land surface temperature products at a semi-desert site. *Proceedings of SPIE*, *5832*, 452–460.

Wang, K., Liu, X., & Sparrow, J. (2005b). Estimating surface solar radiation over complex terrain using moderate-resolution satellite sensor data. *International Journal of Remote Sensing*, *26*(1), 47–58.

Wang, K., Wan, Z., Wang, P., Sparrow, M., Liu, J., Zhou, X., et al. (2005c). Estimation of surface long wave radiation and broadband emissivity using moderate resolution imaging spectroradiometer (MODIS) land surface temperature/emissivity products. *Journal of Geophysical Research*, *110* (D11109). doi:10.1029/2004JD005566.

Wang, K., Zhou, X., Li, W., Liu, J., & Wang, P. (2005d). Using satellite remotely sensed data to retrieve sensible and latent heat fluxes: A review.*Advance in Geoscience*, *20*(1), 42–48 (in Chinese with English abstract).

Yunusa, I. A. M., Walker, R. R., & Lu, P. (2004). Evapotranspiration components from energy balance, sapflow and microlysimetry techniques for an irrigated vineyard in inland Australia. *Agricultural and Forest Meteorology*, *127*, 93–107.

Zhang, Y., Rossow, W. B., Lacis, A. A., Oinas, V., & Mishchenko, M. I. (2004). Calculation of radiative fluxes from the surface to top of atmosphere based on ISCCP and other global data sets: Refinements of the radiative transfer model and the input data. *Journal of Geophysical Research*, *109* (D19105). doi:10.1029/2003JD004457.